

## Microthermometric analysis of synthetic fluid inclusions in the hydrothermal diamond-anvil cell

CHRISTIAN SCHMIDT,<sup>1</sup> I-MING CHOU,<sup>2</sup> ROBERT J. BODNAR,<sup>3,\*</sup> AND WILLIAM A. BASSETT<sup>4</sup>

<sup>1</sup>GeoForschungsZentrum Potsdam, Telegrafenberg D329, Potsdam 14473, Germany

<sup>2</sup>U.S. Geological Survey, 955 National Center, Reston, Virginia 20192, U.S.A.

<sup>3</sup>Fluids Research Laboratory, Department of Geological Sciences, Virginia Polytechnic Institute and State University, Blacksburg, Virginia 24061-0420, U.S.A.

<sup>4</sup>Department of Geological Sciences, Cornell University, Ithaca, New York 14853, U.S.A.

### ABSTRACT

The hydrothermal diamond-anvil cell (HDAC) was employed as a pressurized fluid inclusion heating stage to determine temperatures of phase transitions in synthetic fluid inclusions in quartz. Using this technique, the common problem of decrepitation or stretching of inclusions having high internal pressures was eliminated.

Homogenization temperatures of pure H<sub>2</sub>O synthetic inclusions determined in the HDAC are inversely related to the confining pressure exerted on the sample, suggesting a decrease in inclusion volume with increasing confining pressure. The very good reproducibility and reversibility of these experiments indicate that volume changes during heating under confining pressure in the HDAC are elastic in nature. However, results of microthermometric experiments in the HDAC indicate that the change in homogenization temperature is significantly larger than would be predicted by the equations of state for quartz and water. This difference reflects an additional component of volume change related to stress within the quartz host, causing displacement of the inclusion walls into the inclusion cavity, as predicted by theoretical models describing the behavior of inclusions in minerals.

Liquid-vapor homogenization temperatures [Th(L-V)] and halite dissolution temperatures (T<sub>m</sub> halite) were determined for synthetic fluid inclusions in the ternary H<sub>2</sub>O-NaCl-CO<sub>2</sub>. The measured homogenization temperatures were regressed as a function of confining pressure at Th(L-V). The intersection of the Th(L-V)-confining pressure curve with an independently obtained *P-T* curve for the solvus of the same ternary composition provides the “correct” homogenization temperature, that is, the homogenization temperature corresponding to a confining pressure equal to the pressure on the solvus at that same temperature. This method for determining corrected Th(L-V) is based on the assumption that the effect of elastic stress on Th(L-V) approaches zero as the confining pressure approaches the internal pressure in the inclusion at homogenization. The Th(L-V) values at these intersection points were used to calculate lines of constant homogenization temperature (iso-Th lines). For a composition of H<sub>2</sub>O + 40 wt% NaCl + 10 mol% CO<sub>2</sub>, the iso-Th slopes decrease from about 53 bar/°C at Th(L-V) = 500 °C to 8.5 bar/°C for Th(L-V) = 650 °C. The halite dissolution temperature (in the presence of liquid and vapor) averages 342 °C (range ±6 °C) without recognizable pressure dependence. The slopes of iso-Th lines for a composition of H<sub>2</sub>O + 20 wt% NaCl + 20 mol% CO<sub>2</sub> decrease from approximately 23 bar/°C at Th(L-V) = 475 °C to 6 bar/°C for Th(L-V) = 600 °C.

Using the HDAC technique, the high-pressure portion of the halite liquidus was redetermined for an H<sub>2</sub>O-NaCl solution containing 40 wt% NaCl. These new measurements confirm the data of Bodnar (1994), which were obtained using a gas-flow heating stage at 1 atm confining pressure. This indicates that Bodnar’s (1994) observation of an essentially pressure independent liquidus at pressures  $\geq 2$  kbar is real and not a result of inclusion stretching.

### INTRODUCTION

Typically, fluid inclusion homogenization temperatures are measured in a heating-cooling stage at 1 atm confin-

ing pressure. For inclusions that have relatively low internal pressures at homogenization, homogenization temperatures obtained in this manner are accurate and reproducible and can be used to determine fluid inclusion isochores and, consequently, the conditions of trapping

\* E-mail: bubbles@vt.edu

(Roedder 1984). However, if the fluid inclusion generates a high internal pressure during heating to homogenization, measured homogenization temperatures may be incorrect because of both inelastic and elastic volume changes during heating. For most natural inclusions, errors in isochore location resulting from elastic volume changes are small compared to errors resulting from incompletely known inclusion compositions and can be ignored. For synthetic fluid inclusion studies in which composition and trapping conditions are well known, errors in isochore locations resulting from elastic volume changes can be minimized by using equations of state for the host phase to correct for these volume changes (cf. Bodnar and Sterner 1985; Sterner and Bodnar 1991). Inelastic volume changes, on the other hand, can be very large and lead to significant errors in interpretation of microthermometric data (cf. Larson et al. 1973). In some cases, the inclusion may stretch, leak, or decrepitate before the homogenization temperature is reached. Irreversible volume changes have long been recognized as one of the main problems in microthermometry and have been studied experimentally by numerous workers (e.g., Tugarinov and Naumov 1970; Bodnar and Bethke 1984; Bodnar et al. 1989; Sterner and Bodnar 1989). Bodnar and Bethke (1984) define the various terms used to describe both elastic and non-elastic inclusion volume changes. They defined stretching as a non-elastic volume change that does not include loss of any contents from the inclusions and is accommodated by plastic deformation of the host surrounding the inclusion. More recently, Vityk and Bodnar (1997) have modified this definition based on TEM studies of quartz surrounding stretched inclusions. The modified definition acknowledges the fact that small, undetectable amounts of water are lost from the inclusion by diffusion along dislocations during stretching, and this water in turn promotes plastic deformation of the surrounding quartz. *Decrepitation* describes the process whereby fluid inclusions lose all fluid instantaneously along fractures in the surrounding host. *Leakage* is a form of re-equilibration in which small but measurable amounts of the inclusion contents are lost (e.g., by diffusion or by fracturing of the inclusion walls).

Internal pressures sufficiently high to cause stretching, leakage, or decrepitation of fluid inclusions can be generated in various ways. High internal pressures are most commonly a problem in volatile-rich aqueous inclusions, particularly those that also have moderate to high salinities and high densities. This is due to (1) the steep isochoric  $P$ - $T$  path that the inclusions follow as they are heated through the liquid + vapor  $\pm$  solid region from ambient temperatures and (2) the high solvus (vapor) pressures for these compositions and densities. However, high internal pressures also can be generated by volatile-free inclusions if they are overheated or if the homogenization temperatures are sufficiently high. For example, a pure  $H_2O$ -NaCl inclusion containing 50 wt% NaCl that homogenizes at 700 °C would have an internal pressure of about 1 kbar at homogenization (Bodnar et al. 1985).

It should be noted at this point that use of the units weight percent (wt%) and mole percent (mol%) in this study always refers to the concentration of a component relative to water, e.g., 50 wt% NaCl = [(50 g NaCl)/(50 g NaCl + 50 g water)] $\cdot$ 100. Thus, compositions given for ternary mixtures of  $H_2O$ -NaCl- $CO_2$  described below do not refer to the NaCl or  $CO_2$  bulk concentration.

As a result of irreversible volume changes that occur in response to high internal pressures generated during heating, studies of natural fluid inclusions from many hydrothermal, igneous, and medium- to high-grade metamorphic environments have been hampered (Vityk and Bodnar 1995; Vityk et al. 1994, 1995). Similarly, determinations of isochores and phase equilibria using synthetic fluid inclusions in quartz are generally limited to densities and compositions where the vapor pressure at homogenization is  $\leq$ 2 kbar. This pressure is approximately the internal pressure required to initiate non-elastic deformation of aqueous inclusions 5  $\mu$ m in diameter in quartz during heating at 1 atm confining pressure (Bodnar et al. 1989). Smaller inclusions can withstand significantly larger internal pressures, but visual observation of phase transitions in such small inclusions is often difficult or impossible. Additionally, interpretations of phase transitions observed in small inclusions with high internal pressures may have large uncertainties if the phase transition has a large pressure dependence (Sterner and Bodnar 1991; Bodnar 1994).

Poland (1982) reported that when fluorite was overheated under a confining pressure in a cold-seal pressure vessel, initiation of stretching of fluid inclusions occurred at higher temperatures (compared to overheating at 1 atm). Later, Dahan et al. (1986) described a pressurized heating stage that permitted microscopic determination of phase transition temperatures at confining pressures up to 1 kbar. They reported that when natural fluid inclusions in fluorite were overheated under different confining pressures, the amount of overheating required to initiate stretching increased as the confining pressure increased. Furthermore, these workers noted a slight inverse correlation between homogenization temperature and confining pressure for unstretched aqueous inclusions in fluorite, although the magnitude of this effect was very close to the experimental error of the temperature measurements. These workers were unable to interpret these observations in terms of the relationship between confining pressure and density (or volume) change because they did not know the composition of the inclusions and, thus, did not know the  $P$ - $V$ - $T$  behavior of the inclusion fluid.

The results of these early studies suggested that if a high hydrostatic confining pressure could be applied to the sample during heating, stretching, or decrepitation of inclusions with high internal pressures could be eliminated or at least minimized. Recently, Bassett et al. (1993) described a hydrothermal diamond-anvil cell (HDAC), which could be used to generate hydrostatic pressures up to 25 kbar. This cell was designed to be used on a petrographic microscope so that the pressurized sam-

ple chamber could be observed at high magnification during heating. The feasibility of using the HDAC in fluid inclusion research was first evaluated by measuring halite-dissolution temperatures of 40 wt% NaCl synthetic fluid inclusions in quartz (J. Mavrogenes, R. Bodnar, and I-Ming Chou, 1993, unpublished data), and the methodology was described by Chou et al. (1994). In this paper, we present the results of the first successful application of the HDAC to obtain accurate microthermometric data from fluid inclusions that develop high internal pressures during heating to homogenization. Furthermore, we quantitatively evaluate the effect of elastic volume changes that occur during measurements at high confining pressures.

## METHODS

### Fluid inclusion synthesis

All fluid inclusions examined in this study were synthetic inclusions in natural quartz. Fluid inclusion synthesis followed the procedure described in detail by Bodnar and Sterner (1987) and Sterner and Bodnar (1991). Synthetic fluid inclusions selected for this study consisted of the following compositions within the ternary system water-sodium chloride-carbon dioxide:

- (1)  $X_{(\text{H}_2\text{O})} = 1$ ;
- (2)  $X_{(\text{H}_2\text{O})} = 0.8295$ ,  $X_{(\text{NaCl})} = 0.1705$   
(40 wt% NaCl relative to water);
- (3)  $X_{(\text{H}_2\text{O})} = 0.7595$ ,  $X_{(\text{NaCl})} = 0.1561$ ,  
 $X_{(\text{CO}_2)} = 0.0844$   
(40 wt% NaCl and 10 mol%  $\text{CO}_2$ , both relative to water);
- (4)  $X_{(\text{H}_2\text{O})} = 0.7535$ ,  $X_{(\text{NaCl})} = 0.0581$ ,  
 $X_{(\text{CO}_2)} = 0.1884$   
(20 wt% NaCl and 20 mol%  $\text{CO}_2$ , both relative to water).

Samples containing pure water and  $\text{H}_2\text{O}$ -NaCl- $\text{CO}_2$  inclusions (compositions 1, 3, and 4) were synthesized as part of a more extensive study of phase equilibria and volumetric properties in this ternary system (Schmidt et al. 1995; Schmidt 1997). Fluid inclusions of composition 2 were synthesized for an earlier study of the halite liquidus and isochores of  $\text{H}_2\text{O} + 40$  wt% NaCl (Bodnar 1994).

Platinum capsules were loaded with a prefractured quartz core, along with  $\text{H}_2\text{O}$ , silver oxalate (as a source of  $\text{CO}_2$ ), and halite or an aqueous sodium chloride standard solution, to give the desired fluid composition. The sealed capsules were placed in cold-seal pressure vessels and run for a few days to four weeks at the  $P$  and  $T$  of interest (2–6 kbar and 400–700 °C). During that time, fluid inclusions were trapped by healing fractures in the

quartz or by precipitating quartz as an overgrowth on the core. After experiment completion, the pressure vessels were cooled approximately isochorically. The quartz cores were then removed from the capsules and cut into disks  $\approx 1$  mm thick, which were polished on both sides and examined petrographically.

### Microthermometric measurements

One part of each sample was used for conventional microthermometry on a Fluid Inc. adapted USGS gas-flow heating-freezing stage (Werre et al. 1979), where the sample is at atmospheric confining pressure. The thermocouple of that stage was calibrated against the  $\text{CO}_2$  triple point ( $-56.6$  °C), and the triple point ( $0.0$  °C) and critical point of water ( $374.1$  °C) using synthetic fluid inclusion standards (Sterner and Bodnar 1984). The accuracy of these temperature measurements ranges from about  $\pm 0.2$  °C at  $-60$  °C, to approximately  $\pm 0.1$  °C for temperatures between  $-20$  and  $+30$  °C, to better than  $\pm 2$  °C for temperatures between 100 and 400 °C. The 1 atm microthermometric analyses were undertaken to verify the inclusion composition and to test for homogeneity of the samples, based on the consistency of appropriate phase changes, using criteria described by Sterner and Bodnar (1984), Bodnar et al. (1985), Bodnar and Sterner (1987), and Schmidt (1997). Measurements using the gas-flow stage also provided an approximation of the maximum temperature that fluid inclusions of a given composition, density, and size could be heated to 1 atm before they began to stretch or decrepitate.

Some of the remaining fluid inclusion disks were thinned to  $\approx 100$ – $200$   $\mu\text{m}$ , placed under a drop of water or alcohol, and broken into small pieces using a diamond-tip cutter. Fragments having diameters  $\leq 450$   $\mu\text{m}$  (or  $\leq 700$   $\mu\text{m}$ , depending on which gasket size was used in the HDAC), which contained fluid inclusions of at least 20  $\mu\text{m}$  with optically discernible phases inside them, were selected for HDAC analyses. The minimum inclusion size was constrained by the fact that the highest magnification objective that could be used with the HDAC in this study was 32 $\times$ , and phase transitions in inclusions smaller than about 20  $\mu\text{m}$  could not be determined with sufficient accuracy at this magnification.

A HDAC, designed and constructed by Bassett et al. (1993), was used for all heating experiments above 1 atm confining pressure. Figure 1 shows a schematic diagram of the sample chamber and heating elements of the HDAC. The core of the cell consists of upper and lower diamond anvils mounted on tungsten carbide seats, molybdenum heating coils wrapped around the tungsten carbide seats, and individual chromel-alumel thermocouples in contact with both the upper and lower diamonds. The heater wires are embedded in ceramic cement that is also used to mount the diamond anvils on the tungsten carbide seats. The thermocouples were calibrated against the 1 atm melting points of azobenzene ( $68$  °C), sodium nitrate ( $306.8$  °C), and sodium chloride ( $801$  °C). A potentiometer is used to control the power supplied to the heating

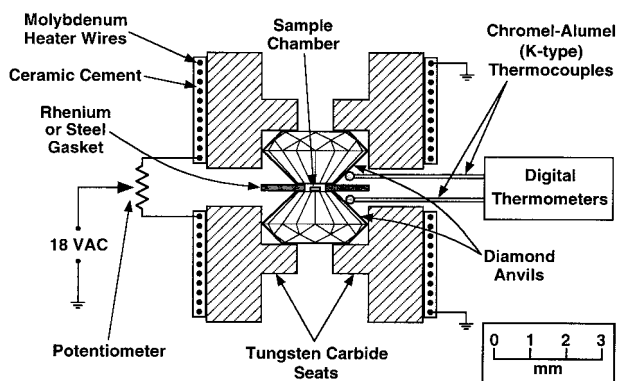


FIGURE 1. Schematic diagram showing the hydrothermal diamond-anvil cell design of Bassett et al. (1993). Adapted from Chou et al. (1994).

coils so that upper and lower thermocouples read the same temperature, thus minimizing vertical thermal gradients. Due to the very small diameter of the sample chamber ( $\approx 0.5$  mm) and the high heat conductivity of diamond, horizontal temperature gradients are low even at high temperatures. A difference of only one degree was measured for the melting point of halite ( $801^\circ\text{C}$ ) from the margin to the center of the chamber. The agreement between homogenization temperatures of pure  $\text{H}_2\text{O}$  fluid inclusion standards measured at 1 atm in the HDAC and in a gas-flow heating stage was generally within  $\pm 1^\circ\text{C}$ . Based on the estimate of Shen et al. (1993), temperatures in the HDAC are accurate to  $\pm 2^\circ\text{C}$ .

The anvils, gasket, seats, thermocouples, and molybdenum heating wires of the HDAC (shown in Fig. 1) are enclosed in a stainless steel cylinder. During heating experiments, flow of an argon-1% hydrogen mixture into the cylinder enclosing the cell prevents oxidation of diamonds and metallic parts. The tungsten carbide seats, along with ceramic heat barriers and mechanisms for anvil alignment, are mounted on an upper and a lower platen that are connected by three posts. Pressure can be applied to the anvils by tightening nuts on the threaded parts of the posts.

The diamond-anvil faces are separated by a rhenium or steel gasket. The sample chamber consists of a circular hole (diameter  $500\text{--}800\ \mu\text{m}$ ) in the gasket that has an uncompressed thickness between  $125$  and  $380\ \mu\text{m}$  ( $250\ \mu\text{m}$  for most experiments). A seal is produced by compressing the gasket between the two diamond-anvil faces. Steel gaskets were used for experiments at lower pressures and temperatures ( $\leq 5$  kbar and  $500^\circ\text{C}$ ). Rhenium was the preferred gasket material for higher pressure experiments because of its better mechanical strength. Initial experiments were conducted using a HDAC having anvil faces of  $\approx 1$  mm in diameter, which limited the diameter of the sample chamber to  $< 500\ \mu\text{m}$ . This necessitated the use of quartz platelets  $< 300\text{--}400\ \mu\text{m}$  in longest dimension, and preparation and loading of such small samples proved to be tedious and time consuming. To

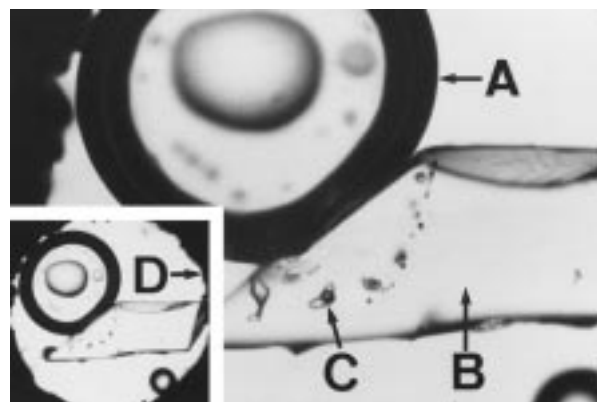


FIGURE 2. Plan view of the sample chamber viewed through the hole in the rhenium gasket at room temperature. The chamber contains water, an air bubble (A), and a doubly polished quartz platelet (B) containing  $\text{H}_2\text{O} + 40\ \text{wt}\% \text{NaCl} + 10\ \text{mol}\% \text{CO}_2$  synthetic inclusions (C). The inset in the lower left shows the sample chamber at lower magnification. The sample chamber diameter is  $\approx 500\ \mu\text{m}$ . (D) rhenium gasket.

facilitate the sample loading process, diamonds with a larger anvil face diameter ( $1.6$  mm) were used in a later version of the cell, which increased the sample chamber diameter to  $\approx 800\ \mu\text{m}$ . Experiments using the HDAC with larger anvil faces were successful, but resulted in a higher pressure on the back side of the anvils. This caused increased wear on the tungsten carbide seats and frequent brittle failure of the ceramic heat barriers, which are located on the back side of the tungsten carbide seats. The hydrothermal diamond-anvil cell was mounted on a microscope stage equipped with video equipment to record phase transitions observed in the sample chamber.

In this study, the chamber of the HDAC was first loaded with a polished  $100\text{--}200\ \mu\text{m}$  thick quartz chip containing fluid inclusions (Fig. 2). Transfer of the quartz chip into the chamber was achieved by sticking a sharpened needle into "Playdough" and wiping the excess from the needle. The needle was then touched to the chip, which would adhere to the needle, and the chip was transferred into the chamber. A small amount of  $\text{H}_2\text{O}$  that served as the pressure medium was then loaded using a  $5\ \mu\text{L}$  syringe. The amount of  $\text{H}_2\text{O}$  added was less than that needed to fill the chamber, resulting in an air bubble in the chamber when it was first sealed at room temperature (Fig. 2).

During microthermometric analysis of fluid inclusions in the HDAC, it is necessary to control the external (confining) pressure in the cell and to know the pressure at any point along the heating path. The pressure must be known because the measured homogenization temperature of a fluid inclusion in the HDAC is dependent on the confining pressure, as described below. Additionally, previous studies have shown that the internal overpressure required to initiate non-elastic deformation of an inclusion depends on the inclusion size (Bodnar et al. 1989). Therefore, care was taken at all times to maintain the

pressure in the sample chamber such that the internal pressure in the inclusion never exceeded the confining pressure in the sample chamber by more than the amount needed to initiate non-elastic deformation. This pressure difference was estimated from the inclusion size using Equation 2 from Bodnar et al. (1989). All of the inclusions studied here were smaller than 100  $\mu\text{m}$  in longest dimension (average  $\approx 30 \mu\text{m}$ ). The inclusion overpressure needed to stretch or decrepitate inclusions 100  $\mu\text{m}$  in diameter is  $\approx 600$  bars, and is  $\approx 1$  kbar for an inclusion 30  $\mu\text{m}$  in diameter (Bodnar et al. 1989). The pressure in the cell is determined from the density (isochore) of the pressure medium ( $\text{H}_2\text{O}$ ), and this value in turn can be controlled by adjusting the degree of fill (water/air bubble ratio) of the sample chamber at room temperature.

Figure 3 shows a schematic  $P$ - $T$  path followed by an  $\text{H}_2\text{O}$ - $\text{NaCl}$ - $\text{CO}_2$  inclusion during heating from room temperature to some temperature above the temperature of homogenization of the fluid inclusion. Assuming a constant inclusion volume as a first approximation, this path is defined by the isochore corresponding to the inclusion bulk density. The inclusion homogenizes when this isochore intersects the solvus (heavy solid line; Fig. 3). At the inclusion homogenization temperature [ $\text{Th}(\text{L-V})_{\text{H}_2\text{O}-\text{NaCl}-\text{CO}_2}$ ; Fig. 3], the pressure in the inclusion is equal to the pressure on the  $\text{H}_2\text{O}$ - $\text{NaCl}$ - $\text{CO}_2$  solvus. With continued heating, the inclusion will follow the isochore into the one-phase field and through the formation conditions ( $T_f$  = formation temperature;  $P_f$  = formation pressure) of the inclusion. It should be kept in mind that the actual  $P$ - $T$  path of the inclusion is slightly nonisochoric. This is due to the compressibility and thermal expansion of the host material, the finite and variable solubility of the quartz host in the inclusion fluid, and elastic volume changes related to the anisotropic behavior of quartz under stress (Zhang 1997, 1998).

The  $P$ - $T$  path of the pressure medium ( $\text{H}_2\text{O}$ ) in the HDAC is determined by the liquid-vapor curve of pure  $\text{H}_2\text{O}$  (heavy dashed line; Fig. 3) as it is heated from room temperature to the temperature at which the vapor ("air") bubble in the sample chamber dissolves. By adjusting the air/water ratio in the cell at room temperature, the temperature at which the water completely fills the cell [ $\text{Th}(\text{L-V})_{\text{H}_2\text{O}}$ ; Fig. 3] can be controlled. With continued heating above that temperature, the  $P$ - $T$  path of the pressure medium follows the isochore (thin dashed line; Fig. 3) corresponding to the  $\text{H}_2\text{O}$  liquid-vapor homogenization temperature [ $\text{Th}(\text{L-V})_{\text{H}_2\text{O}}$ ]. Thus, the confining pressure on the sample at any temperature of interest can be calculated from the  $P$ - $V$ - $T$  properties of  $\text{H}_2\text{O}$ . However, isochoric behavior of the pressure medium can be assumed only if the volume of the sample chamber remains constant and the solubilities of gasket material and inclusion host mineral in water are insignificant.

In this study, the sample chamber pressure was determined by measuring the homogenization temperature of the water in the HDAC (that is, the temperature at which the "air" bubble disappeared) both before and after the

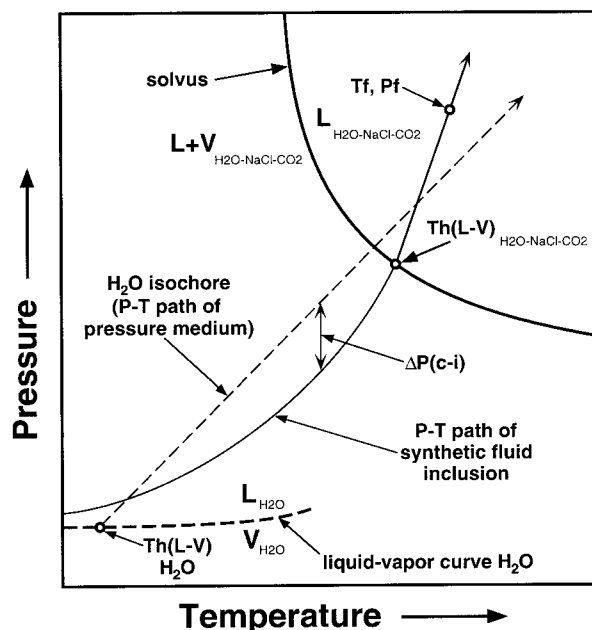


FIGURE 3. Schematic pressure-temperature diagram showing the  $P$ - $T$  paths followed by the water pressure medium and by an  $\text{H}_2\text{O}$ - $\text{NaCl}$ - $\text{CO}_2$  synthetic fluid inclusion in the HDAC. Thin solid line =  $P$ - $T$  path (isochore) of the inclusion;  $\text{Th}(\text{L-V})_{\text{H}_2\text{O}-\text{NaCl}-\text{CO}_2}$  = homogenization temperature of the inclusion; heavy solid line =  $\text{H}_2\text{O}$ - $\text{NaCl}$ - $\text{CO}_2$  solvus corresponding to the inclusion composition;  $L_{\text{H}_2\text{O}}$  = liquid water;  $V_{\text{H}_2\text{O}}$  = water vapor;  $L+V_{\text{H}_2\text{O}-\text{NaCl}-\text{CO}_2}$  = coexisting liquid and vapor in the  $\text{H}_2\text{O}$ - $\text{NaCl}$ - $\text{CO}_2$  ternary;  $L_{\text{H}_2\text{O}-\text{NaCl}-\text{CO}_2}$  = homogeneous liquid in the  $\text{H}_2\text{O}$ - $\text{NaCl}$ - $\text{CO}_2$  ternary;  $T_f$  = inclusion formation temperature;  $P_f$  = inclusion formation pressure; heavy dashed line = liquid-vapor curve of pure water;  $\text{Th}(\text{L-V})_{\text{H}_2\text{O}}$  = water liquid-vapor homogenization temperature = disappearance temperature of the air bubble in the sample chamber; thin dashed line = the  $P$ - $T$  path of the pressure medium (isochore corresponding to  $\text{Th}(\text{L-V})_{\text{H}_2\text{O}}$ );  $\Delta P(\text{c-i})$  = difference between confining pressure on the sample and internal pressure in the inclusion. See text for details.

heating experiment. Owing to the high pressures and temperatures generated during the experiments, stretching and expansion of the gasket sometimes occurred, producing a substantial change in sample chamber volume. This problem was particularly evident when steel gaskets were used. When these gaskets are heated to temperatures  $\geq 500^\circ\text{C}$ , the gasket was observed to creep inward during heating, resulting in a noticeably smaller sample chamber diameter at high temperature compared to room temperature. Upon cooling, the diameter appeared to remain the same as it was at high temperature. This is consistent with the results of a laser interferometric study of the  $\alpha$ - $\beta$  quartz transition up to  $850^\circ\text{C}$  and 11 kbar in a diamond-anvil cell, using somewhat smaller rhenium gaskets than those utilized here (Shen et al. 1993). Only a very small change in pressure medium density occurred upon cooling from the quartz transition temperature to room temperature in that study. In the present study, if the homogenization temperature of the pressure medium in the cell

was the same after heating to high temperatures as it was before being heated, an isochoric heating path was assumed and the external pressure at the phase transition temperature of the fluid inclusion was calculated using the equation of state for pure H<sub>2</sub>O from Haar et al. (1984). If the *P-T* path of the pressure medium drifted significantly toward another isochore during heating, the heating experiment was repeated several times at a lower H<sub>2</sub>O density until no change in the homogenization temperature was observed. A lower H<sub>2</sub>O density was achieved by cooling the HDAC to ambient temperature, loosening the nuts that push the diamond anvils together, and slowly leaking some H<sub>2</sub>O out of the chamber.

By selecting the appropriate filling temperature, the H<sub>2</sub>O *P-T* path will pass through the *P* and *T* of homogenization of the inclusion being measured. Thus, the confining pressure in the cell at the fluid inclusion homogenization temperature will be identical to the pressure in the inclusion at that temperature. The significance of this experimental condition will be discussed in a following section of this paper. In practice, it is too tedious and time consuming to adjust the pressure medium density accurately to a particular value. A less time-consuming procedure is to measure Th(L-V) of the inclusion at several different confining pressures and then to calculate which Th(L-V) corresponds to the solvus pressure, as described below.

## RESULTS AND DISCUSSION

Synthetic fluid inclusions having four different bulk compositions were studied: (1) Pure water inclusions were used to obtain information on the effect of confining pressure on measured inclusion phase transition temperatures. (2) H<sub>2</sub>O + 40 wt% NaCl + 10 mol% CO<sub>2</sub> and H<sub>2</sub>O + 20 wt% NaCl + 20 mol% CO<sub>2</sub> inclusions were examined as part of a more extensive study of phase equilibria and volumetric properties in this ternary system (Schmidt et al. 1995; Schmidt and Bodnar, in preparation). (3) H<sub>2</sub>O + 40 wt% NaCl inclusions were examined to determine halite liquidus temperatures at high pressures. These experiments were carried out to test the hypothesis that the apparent curvature of the liquidus at pressures above ≈2 kbar observed in an earlier study was due to stretching of the inclusions.

### Pure H<sub>2</sub>O inclusions

The first issue that we had to address was the effect of confining pressure on the measured homogenization temperature of a fluid inclusion. This was accomplished by selecting a pure H<sub>2</sub>O synthetic fluid inclusion with a known homogenization temperature in a 1 atm stage. The homogenization temperature of this same inclusion was then measured in the HDAC at different confining pressures. A pure H<sub>2</sub>O inclusion in quartz is ideal for this test because the *P-V-T* properties of H<sub>2</sub>O and quartz, and the solubility of quartz in H<sub>2</sub>O, are well known over the *P-T* range of the experiment. This allowed us to interpret the changing homogenization temperature in terms of a vol-

ume change of the fluid inclusion as a function of confining pressure.

The sample containing pure H<sub>2</sub>O inclusions was synthesized at 500 °C and 4 kbar. The molar volume of pure H<sub>2</sub>O at the formation conditions is 21.693 cm<sup>3</sup>/mol. If the inclusion path from formation conditions to homogenization conditions (and vice versa) is completely isochoric, an inclusion formed at 500 °C and 4 kbar would homogenize on the liquid-vapor curve at 227.6 °C and have an internal pressure of 26.8 bars (Haar et al. 1984). However, the average measured homogenization temperature of the inclusions formed at 500 °C and 4 kbar was 222 ± 1 °C (obtained using a gas-flow heating stage at 1 atm confining pressure). At that temperature and the corresponding liquid-vapor curve pressure of 24.1 bar, the molar volume of H<sub>2</sub>O is 21.504 cm<sup>3</sup>/mol (Haar et al. 1984). The difference between the observed and measured homogenization temperatures can be accounted for by considering the change in the volume of the quartz host during heating and cooling. The molar volume of the host mineral quartz decreases by 0.233% over the *P-T* range from 500 °C and 4 kbar to 222 °C, 24.1 bar. The molar volume of H<sub>2</sub>O, corrected to account for this combined volume change of quartz from thermal expansion and compressibility, is 21.554 cm<sup>3</sup>/mol, which corresponds to a temperature on the H<sub>2</sub>O liquid-vapor curve of 223.5 °C (Haar et al. 1984). This value is in good agreement with the measured homogenization temperature of 222 ± 1 °C and suggests that most of the difference between the predicted (completely) isochoric homogenization temperature and the observed homogenization temperature is accounted for by thermal expansion and compressibility of quartz. The H<sub>2</sub>O isochore corresponding to this corrected homogenization temperature (223.5 °C) intersects the formation temperature (500 °C) at 4048 bars, and intersects the formation pressure (4 kbar) at 497 °C. That is, if the formation temperature has no error, the observed difference is accounted for by a pressure error of 48 bars. Similarly, if the formation pressure has no error, the observed difference is accounted for by a formation temperature error of -3 °C. These small deviations are well within the range of experimental errors in formation temperatures and pressures for experiments conducted in cold-seal pressure vessels (typically ±5 °C and ±50 bars). This observation is also consistent with previous synthetic fluid inclusion studies (Bodnar and Sterner 1985; Sterner and Bodnar 1991), which indicate that the effect of quartz solubility (Fournier and Potter 1982) on H<sub>2</sub>O isochores is small at *P-T* conditions ranging from 1–6 kbar and 300–700 °C, and can be ignored when correcting synthetic fluid inclusion volumes or densities.

As expected, the homogenization temperature was found to be inversely related to the pressure exerted on the quartz platelet hosting the inclusion (Fig. 4), owing to the compression of the quartz host and the concomitant decrease in the inclusion volume. The magnitude of the homogenization temperature shift of the pure H<sub>2</sub>O fluid inclusion shown in Figure 4 is much larger than the un-

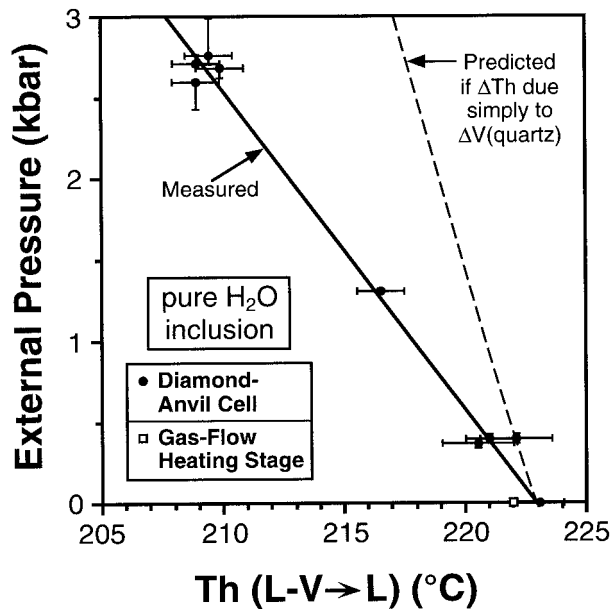


**FIGURE 4.** Homogenization temperature [ $T_h(L-V \rightarrow L)$ ] of the same pure  $H_2O$  inclusion as a function of external hydrostatic pressure on the host. The solid line was obtained by linear regression of the data measured using a hydrothermal diamond-anvil cell (filled circles). Error bars along the x axis express the uncertainty in measuring the homogenization temperature of the inclusion. The error in external pressure was calculated from the uncertainty and observed range of pressure medium homogenization temperatures. The dashed line shows the calculated shift in  $T_h(L-V \rightarrow L)$  assuming that the change in fluid inclusion volume is only related to the change in molar volume of the quartz with pressure and temperature. The equations of state for quartz (Hosieni et al. 1985) and for  $H_2O$  (Haar et al. 1984) were used to calculate the location of the dashed line. The homogenization temperature measured using a conventional gas-flow heating stage (open square) is in very good agreement with the HDAC datum point at 1 atm confining pressure (solid circle at  $P = 0$ ).

certainty of the temperature measurements ( $\pm 1.5^\circ C$ ) and therefore cannot be attributed to temperature measurement errors. Likewise, other possible contributions to the observed  $T_h(L-V)$  shift, such as  $H_2O$  diffusion into quartz or dissolution and precipitation of host material in the fluid inclusion  $H_2O$ , are insignificant at these relatively low temperatures. For example, the difference in quartz solubility in  $H_2O$  along the three phase curve  $H_2O$  (vapor)- $H_2O$  (liquid)-quartz is only about 46 ppm  $SiO_2$  between 223 and 210  $^\circ C$  (Rimstidt 1997), and cannot be the cause of the observed  $T_h(L-V)$  shift.

The shift in  $T_h(L-V \rightarrow L)$  with confining pressure is reversible and reproducible. Experiments at various confining pressures were repeated three times using the same inclusion. In every case, the homogenization temperatures (at about the same confining pressures) showed no deviation in excess of the experimental error of the temperature measurements (Fig. 4). The 1 atm homogenization temperature of the pure  $H_2O$  inclusion was determined in the HDAC (using an air-filled gasket) before

and after the heating experiments at higher confining pressures to check the reproducibility of our data. The sample containing the inclusion was subjected to confining pressures up to about 3 kbar and temperatures of approximately 220  $^\circ C$  for 2–3 hours. No change in the 1 atm homogenization temperature of the pure  $H_2O$  inclusion was detected after completion of the experiments at elevated pressures in the HDAC, suggesting that non-elastic volume changes are not associated with the observed homogenization temperature changes.

The homogenization temperature of an inclusion containing pure  $H_2O$  is very sensitive to small changes in molar volume. At the temperatures of these experiments, the change in the molar volume of  $H_2O$  along the liquid-vapor curve is about  $0.03 \text{ cm}^3/\text{mol}\cdot^\circ C$  (Haar et al. 1984). Thus, even a small amount of plastic deformation without optically noticeable movement of the inclusion walls or change in vapor bubble diameter should be reflected by a recognizable difference in measured  $T_h(L-V \rightarrow L)$ . For example, a volume decrease of only 0.7% at 223  $^\circ C$  would change the homogenization temperature to 218  $^\circ C$ . Non-elastic volume changes, as might be manifest as measurable homogenization temperature changes, were not observed. This lack of a temperature change is probably due to the relatively low temperatures of the experiments and the duration of loading (less than a few hours), which was too short to trigger movement along dislocations on inclusion walls (Poirier 1985; Vityk et al. 1994). The small difference of about 1  $^\circ C$  between the 1 atm homogenization temperature measured in a gas-flow stage and that measured in the HDAC is within the attainable accuracy of temperature measurements using these heating stages and should not be attributed to stretching. Based on the reproducibility of the measured  $T_h(L-V \rightarrow L)$ , there is no evidence for non-elastic volume changes, and our interpretation of the homogenization temperature data assumes only elastic behavior of the inclusion-host system during analysis in the HDAC.

The results of experiments on synthetic pure  $H_2O$  inclusions in the HDAC indicate that the inclusion density changes by an amount greater than would be predicted by the volume change of the quartz host resulting from thermal expansion and compressibility alone. The dashed and solid lines in Figure 4 compare the predicted and observed inclusion density, expressed as the shift in  $T_h(L-V)$  with external pressure. Assuming hydrostatic pressure on the quartz platelet, the volume change of quartz over the range from 222.9  $^\circ C$ , 1 bar to 210  $^\circ C$ , 2535 bars is  $-0.8\%$  (Hosieni et al. 1985). The pressure of 2535 bars represents the confining pressure on the sample at 210  $^\circ C$  based on a linear regression of the experimental data plotted in Figure 4.

The volume change of the inclusion with confining pressure is easily calculated from the measured homogenization temperature and  $P$ - $V$ - $T$  properties of  $H_2O$ . The internal pressure and the molar volume of the inclusion at homogenization are fixed for a given temperature on the liquid-vapor curve of  $H_2O$ . Based on the equation of

Haar et al. (1984), the pressure in the inclusion decreases from 24.5 bar for  $T_h(L-V) = 222.9^\circ\text{C}$  to 19.1 bar at  $T_h(L-V) = 210^\circ\text{C}$ . Over that  $P$ - $T$  interval, the molar volume of the inclusion decreases by 1.9%, which is more than twice the volume change predicted over the same  $P$ - $T$  interval from the equation of state of quartz. The considerable anisotropy of quartz compressibility (Angel et al. 1997) and thermal expansion cannot explain why the observed shift in inclusion density with confining pressure is greater than predicted. This is because the change in inclusion volume does not depend on its shape or crystallographic orientation because the volume change of a given number of quartz unit cells is the same regardless of whether these unit cells are stacked along the  $a$  axis or the  $c$  axis.

One possible explanation for this anomalous behavior is that the stress distribution in the host mineral around an inclusion must be taken into account if host and inclusion are at different average pressures (Zhang 1997). Calculations show that "for spherical concentric inclusion and host that are isotropic, the inclusion is always under uniform hydrostatic pressure, whereas the host can be under substantial deviatoric stress and variable average pressure" (Zhang 1997). Even at elastic equilibrium between host and fluid inclusion, stress effects will cause displacements of the inclusion walls into the inclusion cavity with increasing confining pressure. This inclusion volume decrease is in addition to the displacement of the inclusion walls due to the compressibility of quartz. If elastic anisotropy of the host is taken into consideration, the calculated volume of a spherical pure  $\text{H}_2\text{O}$  inclusion in quartz decreases by 1.8% over the same temperature interval and corresponding internal and confining pressures, as given in the preceding paragraph (Zhang 1998). This value is in good agreement with the observed  $-1.9\%$  volume change. The pure  $\text{H}_2\text{O}$  inclusion used in this study was fairly equant and  $\approx 30\ \mu\text{m}$  in diameter. The volume change of an inclusion with confining pressure should also be slightly dependent on inclusion size (Zhang 1998). We were not able to verify this dependence experimentally because the range in the size of the inclusions used for measurements in the HDAC was relatively small ( $\approx 20$ – $100\ \mu\text{m}$ ).

#### Interpretation of thermometric data obtained at a confining pressure $>1\ \text{atm}$

Considerable shifts in homogenization temperature with external pressure were not only observed for pure  $\text{H}_2\text{O}$  inclusions but also for other fluid inclusion compositions ( $\text{H}_2\text{O} + 40\ \text{wt}\% \text{NaCl}$ ,  $\text{H}_2\text{O} + 40\ \text{wt}\% \text{NaCl} + 10\ \text{mol}\% \text{CO}_2$ ,  $\text{H}_2\text{O} + 20\ \text{wt}\% \text{NaCl} + 20\ \text{mol}\% \text{CO}_2$ ). The largest shift measured in this study was about  $11^\circ\text{C}/\text{kbar}$  external pressure. Figure 5 shows the effect of the homogenization temperature shift ( $\Delta T_h$ ) with external pressure on the calculated inclusion trapping conditions. The homogenization temperature obtained at 1 atm external pressure can differ by several tens of degrees from the homogenization temperature measured at high exter-

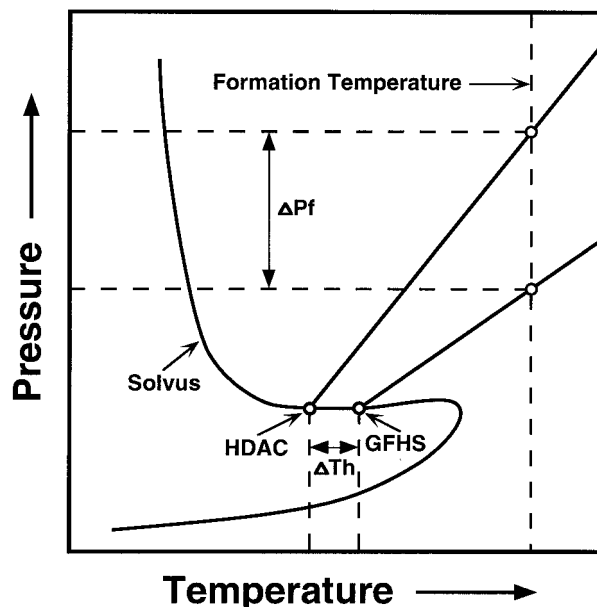


**FIGURE 5.** Schematic  $P$ - $T$  diagram showing the geobarometric consequences of the homogenization temperature shift ( $\Delta T_h$ ) with external pressure. The isochore of a fluid inclusion can be determined from its homogenization temperature and bulk composition. The possible  $P$ - $T$  conditions of inclusion entrapment are located along the isochore. Therefore, the formation pressure can be calculated if the formation temperature is known independently. The homogenization temperature obtained at 1 atm external pressure using a gas-flow heating stage (GFHS) can differ by several tens of degrees from the homogenization temperature measured at high external pressure using a HDAC. A relatively small  $\Delta T_h$  error may result in a large error in the calculated formation pressure ( $\Delta P_f$ ).

nal confining pressure in the HDAC. Moreover, isochore slopes can change considerably with relatively small changes in homogenization temperature. Therefore, a shift in homogenization temperature ( $\Delta T_h$ ) of several tens of degrees may result in a relatively large error ( $\Delta P_f$ ) in the calculated formation pressure when the isochore is extrapolated to a known formation temperature (Fig. 5).

Which homogenization temperature, then, is the correct one to use in fluid inclusion studies conducted in a HDAC? As discussed in the preceding section, homogenization temperatures are a function of confining pressure during the measurements. Moreover, the magnitude of elastic volume changes related to stress on the inclusion walls increases as the difference between confining and internal pressure [ $\Delta P(c-i)$ ] increases (Zhang 1997). The volume change experienced by a fluid inclusion as it cools from trapping conditions to ambient temperature will normally be difficult to recognize if only elastic deformation occurs because  $\Delta P(c-i)$  is zero at trapping and generally small at room temperature for most inclusions. Furthermore, elastic and non-elastic volume changes are minimized if the cooling path of the host is reasonably close to the isochore of the fluid in the inclusion. Thus,

the assumption that natural fluid inclusions do not significantly change their volume after trapping (Roedder 1984) is still a good approximation for many fluid inclusions, particularly those formed in shallow crustal environments. Due to the small  $\Delta P(c-i)$ , heating stages operating at 1 atm confining pressure will yield satisfactory data for inclusions with low internal pressures (less than a few hundred bars) at homogenization. In such cases, application of the HDAC is not required. Evidence for this is provided by the fact that specific volumes of  $H_2O$  obtained from synthetic fluid inclusions reproduce  $P$ - $V$ - $T$  data from other experimental techniques within 1% (Bodnar and Sterner 1985, 1987; Sterner and Bodnar 1991; this study). During heating of fluid inclusions at ambient (1 atm) confining pressure,  $\Delta P(c-i)$  increases as the internal pressure in the inclusion increases with temperature. This results in a shift in the homogenization temperature. The magnitude of this temperature shift is normally just a few degrees Celsius, which is close to the precision of homogenization temperature determinations at high temperatures (several hundred degrees Celsius) using most heating stages.

Compared to microthermometric analyses of gas-free, low-density inclusions that develop only low to moderate internal pressures during heating, internal pressures in gas-rich, high-density inclusions can become very high during heating. However, the change in inclusion volume resulting from stress effects on the host is zero if the external (sample chamber) pressure equals the internal pressure in the inclusion. Therefore, the only volume changes that need to be considered are those related to thermal expansion and compressibility of the quartz host. Based on these relationships, the following strategy was used to obtain a "correct" homogenization temperature from HDAC measurements. First,  $Th(L-V)$  of the same inclusion was measured at different confining pressures and the results regressed to give confining pressure as a function of  $Th(L-V)$ . Then, confining pressure was plotted vs.  $Th(L-V)$ , and the  $P$ - $T$  location of the solvus for that particular fluid composition was also plotted on the same diagram (Fig. 6). The temperature at which the confining pressure- $Th(L-V)$  curve intersects the solvus curve thus represents the "correct" homogenization temperature. That is, it represents the homogenization temperature at which the confining pressure and the internal pressure are equal. This approach was used in this study to determine the "correct" homogenization temperatures for  $H_2O$ - $NaCl$ - $CO_2$  inclusions measured in the HDAC.

#### Lines of equal homogenization temperature for $H_2O$ - $NaCl$ - $CO_2$ mixtures

Application of the technique described above for determining the "correct" homogenization temperature requires knowledge of the solvus location in  $P$ - $T$  space for a given fluid composition. While such data exist for most unary and many binary systems, much less is known about phase equilibria in more complex systems. Fortunately, for synthetic fluid inclusions, a good estimate of

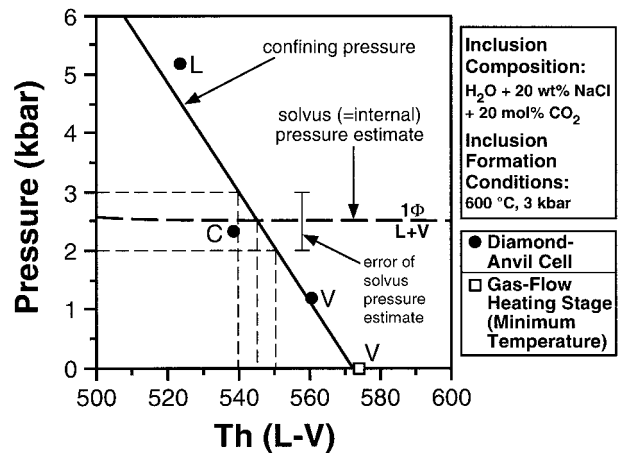


FIGURE 6.  $P$ - $T$  plot illustrating the technique used to determine the "correct" homogenization temperature for a fluid inclusion with a composition of  $H_2O + 20$  wt%  $NaCl + 20$  mol%  $CO_2$ . A portion of the solvus for this composition is shown by the heavy, nearly horizontal dashed line. Filled circles represent homogenization temperatures measured at different confining pressures for the same inclusion using a hydrothermal diamond-anvil cell [L = homogenization to the liquid (aqueous) phase, V = homogenization to the vapor (carbonic) phase, C = homogenization by critical behavior]. The open square represents the homogenization temperature of the same inclusion measured at 1 atm confining pressure. The thick solid line represents a linear fit to the measured  $Th(L-V)$  of the inclusions as a function of confining pressure. The intersection of the confining pressure function with the solvus curve yields a corrected homogenization temperature of  $545 \pm 5.5$  °C at a solvus pressure of approximately  $2.5 \pm 0.5$  kbar.

the liquid-vapor curve location can be obtained independently by bracketing the immiscibility field. Figure 7 illustrates such an estimation of the solvus location for a composition of  $H_2O + 20$  wt%  $NaCl + 20$  mol%  $CO_2$ . Evidence for the presence of a one-phase fluid at the formation conditions is provided by uniformity of phase ratios and consistent aqueous phase salinities and densities of the carbonic phase.  $P$ - $T$  conditions for fluid inclusions showing evidence for trapping in the one-phase field are plotted in Figure 7 as solid circles. Samples run at  $P$ - $T$  conditions within the two-phase field contain inclusions that show a wide range in salinity and  $CO_2$  density and commonly exhibit variable phase ratios at room temperature (Sterner and Bodnar 1984; Bodnar et al. 1985). The  $P$ - $T$  formation conditions of samples showing these characteristics are plotted in Figure 7 as open circles. The  $P$ - $T$  location of the solvus must pass through  $P$ - $T$  conditions that lie between the formation conditions of samples that trapped a homogeneous fluid in the one-phase field and those that trapped an immiscible fluid in the two-phase field. Trapping conditions and microthermometric data for the samples described here are listed in Table 1. Additional experimental details are provided in Schmidt (1997).

At temperatures above 500 °C, the solvus for a com-

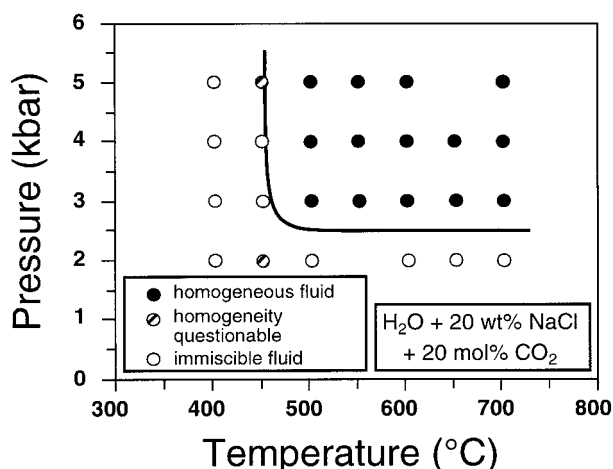


FIGURE 7. Estimated solvus location for the composition  $\text{H}_2\text{O} + 20 \text{ wt}\% \text{ NaCl} + 20 \text{ mol}\% \text{ CO}_2$  based on microthermometric data and petrographic evidence of immiscibility. Circles represent formation conditions of the synthetic fluid inclusion samples. In  $P$ - $T$  space, the solvus must pass through  $P$ - $T$  conditions that lie between the formation conditions of samples that trapped a homogeneous fluid (solid circles) and those that show features characteristic of immiscibility (open circles). See text for more details.

position of  $\text{H}_2\text{O} + 20 \text{ wt}\% \text{ NaCl} + 20 \text{ mol}\% \text{ CO}_2$  is essentially isobaric at about  $2.5 \pm 0.5 \text{ kbar}$  (Fig. 7). On the other hand, the measured homogenization temperatures of high-density inclusions trapped at 500 °C, 4 and 5 kbar, range between 452 and 465 °C and are almost independent of the confining pressure during homogenization in the HDAC. This indicates that the lower temperature portion of the solvus for this composition is located within this temperature interval (452–465 °C) at pressures of approximately 3 to 5 kbar and is essentially

isothermal (Fig. 7). The solvus is thus composed of a higher temperature portion in which the one-phase/two-phase boundary is essentially isobaric and a lower temperature portion where the solvus is essentially isothermal. The  $P$ - $T$  location of the solvus for a composition of  $\text{H}_2\text{O} + 40 \text{ wt}\% \text{ NaCl} + 10 \text{ mol}\% \text{ CO}_2$  was delineated using this same approach and was found to be similar to that of  $\text{H}_2\text{O} + 20 \text{ wt}\% \text{ NaCl} + 20 \text{ mol}\% \text{ CO}_2$  (Fig. 8). The high pressure (3–5 kbar) isothermal portion of the  $\text{H}_2\text{O} + 40 \text{ wt}\% \text{ NaCl} + 10 \text{ mol}\% \text{ CO}_2$  solvus is located at slightly higher temperatures (about  $490 \pm 5 \text{ °C}$ ) compared to that for  $\text{H}_2\text{O} + 20 \text{ wt}\% \text{ NaCl} + 20 \text{ mol}\% \text{ CO}_2$ . For both compositions, the observed shift of  $\text{Th}(\text{L-V})$  with confining pressure is small for inclusions that homogenize along the isothermal portion of the solvus. The shift is significant for inclusions that homogenize along the isobaric portion of the solvus.

For each sample studied, the measured homogenization temperatures were regressed as a function of confining pressure on the sample. These functions were then intersected in  $P$ - $T$  space with the independently obtained solvus for the respective ternary composition as shown on Figure 6. At the intersection, confining pressure equals internal (homogenization) pressure in the inclusion, and the contribution of stress effects on the inclusion walls to the total inclusion volume change is zero (Zhang 1997). Stated differently, stress on the inclusion walls does not affect  $\text{Th}(\text{L-V})$ . Table 1 lists homogenization temperatures of  $\text{H}_2\text{O} + 20 \text{ wt}\% \text{ NaCl} + 20 \text{ mol}\% \text{ CO}_2$  and  $\text{H}_2\text{O} + 40 \text{ wt}\% \text{ NaCl} + 10 \text{ mol}\% \text{ CO}_2$  fluid inclusions for the condition where the internal pressure at homogenization is equal to the confining pressure or solvus pressure [ $\text{Th}(\text{L-V})$  (HDAC) at  $P(\text{solvus})$ ]. The formation temperatures ( $T_f$ ) of the samples were then regressed as a function of these adjusted  $\text{Th}(\text{L-V})$  values using linear equations for each isobar. Lines of constant homogeni-

TABLE 1. Experimental conditions and microthermometric data for  $\text{H}_2\text{O}$ - $\text{NaCl}$ - $\text{CO}_2$  synthetic fluid inclusions

$T_f$ (°C)	$P_f$ (kbar)	NaCl (wt%)	$\text{CO}_2$ (mol%)	$\text{Th}(\text{HDAC})$ (°C)	$P_s$ (kbar)	$n$	$\text{Th}(1 \text{ atm})$ (°C)
500	3.0	20	20	$479 \pm 2$ (L)	2.5	2	466.4 (L)
600	3.0	20	20	$545 \pm 6$ (C,V)	2.5	3	574 (V)
700	3.0	20	20	$608 \pm 10$ (V)	2.5	2	622 (V)
500	4.0	20	20	$461.5 \pm 2$ (L)	3.0	3	n.d.
700	4.0	20	20	$540 \pm 10$ (C,L)	2.5	2	556 (V)
500	5.0	20	20	$455 \pm 3$ (L)	3.5	2	n.d.
600	5.0	20	20.1	$480 \pm 4$ (L)	2.5	6	n.d.
500	3.0	40	10	$490 \pm 5$ (L)	2.8	2	479 (L)
600	3.0	40	10	$579 \pm 5$ (L)	2.5	4	588 (L)
700	3.0	40	10	$656 \pm 5$ (L)	2.5	3	625? (L), 654 (L)
500	4.0	40	10	$488 \pm 7$ (L)	3.7	5	n.d.
600	4.0	40	10	$556 \pm 10$ (L)	2.5	5	571 (L)
700	4.0	40	10	$586 \pm 5$ (L)	2.5	2	608 (L)
500	5.0	40	10	$488 \pm 2$ (L)	4.5	7	n.d.
600	5.0	40	10	$515 \pm 7$ (L)	2.6	4	n.d.
700	5.0	40	10	$559 \pm 10$ (L)	2.5	7	n.d.

Notes:  $T_f$  = formation temperature;  $P_f$  = formation pressure; NaCl (wt%) = NaCl concentration in weight percent relative to  $\text{H}_2\text{O}$ ;  $\text{CO}_2$  (mol%) =  $\text{CO}_2$  concentration in mole percent relative to  $\text{H}_2\text{O}$ ;  $\text{Th}(\text{HDAC})$  = average liquid-vapor homogenization temperature in the HDAC at the estimated solvus pressure; (L) = homogenization to the liquid; (V) = homogenization to the vapor; (C) = homogenization by critical behavior;  $P_s$  = solvus pressure;  $\text{Th}(1 \text{ atm})$  = minimum liquid-vapor homogenization temperature in the gas-flow heating state;  $n$  = number of measured inclusions; n.d. = not determined (due to stretching or decrepitation).

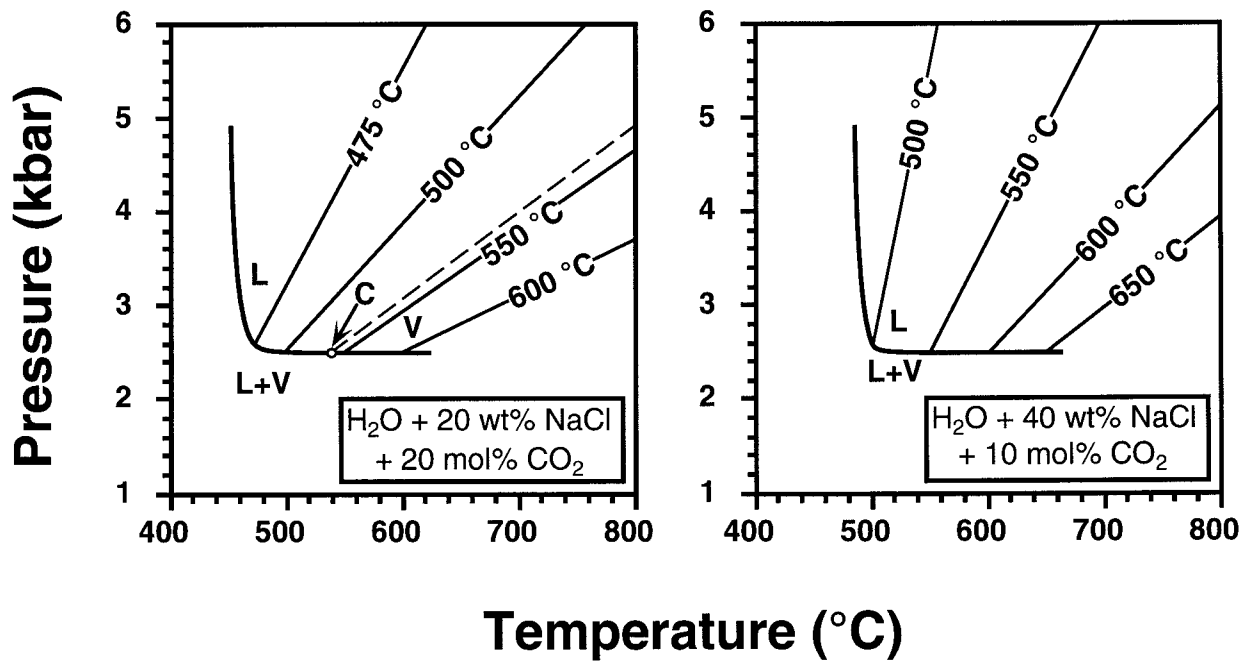
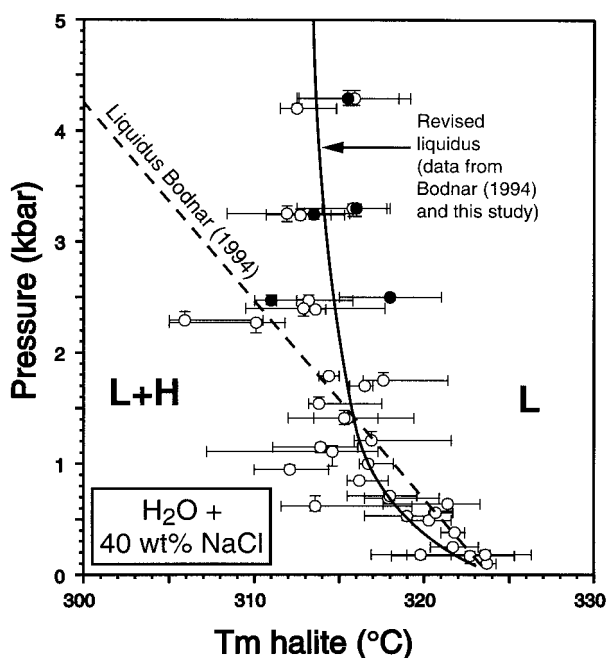


FIGURE 8. Lines of equal homogenization temperature (iso-Th lines) and the high-pressure portion of the solvus of aqueous solutions containing 20 wt% NaCl + 20 mol% CO<sub>2</sub> (left *P-T* diagram) and 40 wt% NaCl + 10 mol% CO<sub>2</sub> (right *P-T* diagram), based on homogenization temperatures normalized to solvus pressures. L+V = liquid-vapor field; L = liquid field (homogenization to the liquid phase); V = vapor field (homogenization to the vapor phase); C = critical point ( $\approx 540$  °C,  $\approx 2.5$  kbar); dashed line = critical isochore separating liquid and vapor fields.

TABLE 2. Halite dissolution temperatures and experimental conditions for synthetic fluid inclusions containing 40 wt% NaCl relative to water

Tf (°C)	Pf (kbar)	NaCl (wt%)	CO <sub>2</sub> (mol%)	Tm halite (HDAC)	P(ext) (kbar)	<i>n</i>	Tm halite (1 atm)	P(lqds) (kbar)
400	5.0	40.00	0	316 ± 1	4.45	3	315.8*	3.30*
400	5.0	40.03	0	313.5	3.53	1	312.7*	3.24*
400	6.0	40.08	0	315.5 ± 2	4.22	3	315.9*	4.29*
500	6.0	39.96	0	311.5	4.50	1	313.2*	2.47*
				311	0.92	1		
500	6.0	40.02	0	318 ± 2	3.9	3		
500	3.0	40	10	N.D.			345.4 (22)	N.D.
600	3.0	40	10	345.5 ± 2	1.86	3	340.9 (20)	N.D.
				343	2.59	1		
				344	3.63	1		
				340	0.36	1		
				339	2.55	1		
				338	3.74	1		
700	3.0	40	10	343	0.15	1	339.5 (27)	N.D.
				341	0.17	1		
				343	1.40	1		
500	4.0	40	10	344 ± 1	0.52	4	344.2 (20)	N.D.
600	4.0	40	10	341.5 ± 1	2.86	2	341.6 (20)	N.D.
700	4.0	40	10	342 ± 1	0.23	3	340.8 (10)	N.D.
				340	2.98	1		
500	5.0	40	10	341.5	2.43	1	340.3 (15)	N.D.
600	5.0	40	10	340 ± 1	1.47	4	339.4 (16)	N.D.
700	5.0	40	10	339	0.26	1	342.7 (19)	N.D.

Notes: Tf = formation temperature; Pf = formation pressure; NaCl (wt%) = NaCl concentration in weight percent relative to H<sub>2</sub>O; CO<sub>2</sub> (mol%) = carbon dioxide concentration in mole percent relative to H<sub>2</sub>O; Tm halite (HDAC) = average halite dissolution temperature in the HDAC at the external pressure given in the next column; P(ext) = calculated external pressure at Tm halite (HDAC); *n* = number of inclusions; Tm halite (1 atm) = average halite dissolution temperature obtained using a gas-flow heating stage, data from Bodnar (1994) indicated by an asterisk (\*); P(lqds) = average liquidus pressure; N.D. = not determined.



**FIGURE 9.** Liquidus pressure of a 40 wt% NaCl aqueous solution as a function of halite dissolution temperatures ( $T_m$  halite). L+H = coexisting liquid and halite; L = liquid field; open circles = data from Bodnar (1994) obtained using a gas-flow heating stage at 1 atm confining pressure; solid circles = halite dissolution temperatures, as determined in this study at high confining pressure using a HDAC. Error bars along the x axis express the range in measured  $T_m$  halite. Error bars along the pressure axis represent the range in liquidus pressures of the samples, as calculated by Bodnar (1994).

zation temperature (iso-Th lines) were then obtained by solving the regression equations corresponding to each isobar at regular integer  $Th(L-V)$  values, e.g.,  $Th(L-V) = 500$  °C, 550 °C, 600 °C, etc.. Thus, solving the “3 kbar” equation for a  $Th(L-V)$  of 500 °C gives the formation temperature needed at 3 kbar to produce fluid inclusions that homogenize at 500 °C. Iso-Th lines calculated in this manner and the solvus for each ternary composition ( $H_2O + 20$  wt% NaCl + 20 mol%  $CO_2$  and  $H_2O + 40$  wt% NaCl + 10 mol%  $CO_2$ ) are shown on Figure 8. The iso-Th line slopes for an  $H_2O + 40$  wt% NaCl + 10 mol%  $CO_2$  mixture decrease from about 53 bar/°C at  $Th(L-V) = 500$  °C to 8.5 bar/°C for  $Th(L-V) = 650$  °C. The iso-Th line slopes of  $H_2O + 20$  wt% NaCl + 20 mol%  $CO_2$  range from approximately 23 bar/°C at  $Th(L-V) = 475$  °C to about 6 bar/°C for  $Th(L-V) = 600$  °C.

The halite dissolution temperatures (in presence of liquid and vapor) of  $H_2O + 40$  wt% NaCl + 10 mol%  $CO_2$  average 342 °C (range  $\pm 6$  °C) and show no recognizable pressure dependence (Table 2). The halite dissolution temperatures for these more  $CO_2$ -rich inclusions are slightly elevated compared to previously determined halite dissolution temperatures for lower  $CO_2$  concentrations along the 40 wt% NaCl pseudobinary (Schmidt et al.

1995). In the binary  $H_2O$ -NaCl, the vapor-saturated halite liquidus for 40 wt% NaCl occurs at 323 °C (Bodnar 1994), whereas the vapor-saturated halite liquidus for a composition of  $H_2O + 40$  wt% NaCl + 5 mol%  $CO_2$  is at 332 °C (Schmidt et al. 1995).

#### Halite liquidus of $H_2O + 40$ wt% NaCl

Aqueous inclusions that contain halite and homogenize by disappearance of the halite crystal after liquid-vapor homogenization can generate high internal pressures during heating (Bodnar 1994), and therefore they are often not suitable for study in a 1 atm heating stage. As a final example of the application of the HDAC in fluid inclusion research, we have measured the halite dissolution temperature of inclusions in the  $H_2O$ -NaCl binary system having liquidus pressures above 2 kbar.

Bodnar (1994) estimated the  $P$ - $T$  position for the halite liquidus of a 40 wt% NaCl solution using homogenization temperatures and halite dissolution temperatures [ $T_m$  NaCl] of synthetic fluid inclusions measured at 1 atm confining pressure. That study showed a decrease in the halite dissolution temperatures from about 323 °C at a calculated liquidus pressure of approximately 100 bars to about 315 °C at a calculated pressure of 1.8 kbar (Fig. 9). At higher pressures, there was little change in the measured  $T_m$  NaCl. Bodnar (1994) calculated the liquidus pressure by finding the pressure at the halite dissolution temperature on the iso-Th line corresponding to the measured homogenization temperature [ $Th(L-V)$ ]. The iso-Th lines were determined by regression of measured  $Th(L-V)$  along formation pressure isobars as a function of formation temperatures of the individual samples (similar to the procedure described in the previous section).

Bodnar (1994) approximated the liquidus using a linear regression of data points with liquidus pressures <2 kbar, assuming that data at higher pressures were shifted toward higher temperatures due to stretching, thus lowering the internal pressure (Fig. 9). To evaluate the effect of stretching, we redetermined the halite dissolution temperatures of five high density  $H_2O + 40$  wt% NaCl samples using the HDAC technique. Four of these samples were studied previously by Bodnar (1994). The confining pressures on the samples measured in the HDAC varied between 0.9 and 4.5 kbar. If the earlier interpretation that  $T_m$  NaCl for inclusions with high calculated pressures was shifted toward higher temperatures due to stretching was correct, we expected to find lower  $T_m$  NaCl for inclusions studied in the HDAC at a high confining pressure. However, the halite dissolution temperatures from both data sets are in very good agreement (Table 2 and Fig. 9). This does not imply that the high-density inclusions measured by Bodnar (1994) were not changed by stretching. The liquidus pressures calculated by Bodnar (1994) are maximum values, i.e., the actual internal pressure in the high-density inclusions at  $T_m$  NaCl during measurements at 1 atm confining pressure was certainly lower than the calculated liquidus pressure. The agreement between the results obtained in the HDAC and the

data of Bodnar (1994; Fig. 4 and Table 1) suggests that the liquidus temperature for this composition is essentially independent of pressure at pressures  $\geq 2$  kbars. Furthermore, the combined results of both studies indicate that the liquidus has a curvature toward lower  $T_m$  NaCl with increasing pressure at liquidus pressures  $\leq 2$  kbar (Fig. 9).

#### ACKNOWLEDGMENTS

This research was sponsored by grants from the Geosciences Program, Office of Basic Energy Sciences, U.S. Department of Energy (DE-FG05-89ER14065) and from the National Science Foundation (EAR-9725248) to R.J.B. The authors thank Ross Angel, Frank Harrison, John Mavrogenes, Don Rimstidt, James Student, Maxim Vityk, and Youxue Zhang for helpful discussions and their support and assistance with various aspects of this study. Reviews by Edwin Roedder, Craig Manning, Dan Harlov, and an anonymous reviewer improved earlier versions of this paper.

#### REFERENCES CITED

- Angel, R.J., Allan, D.R., Miletich, R., and Finger, L.W. (1997) The use of quartz as an internal pressure standard in high-pressure crystallography. *Journal of Applied Crystallography*, 30, 461–466.
- Bassett, W.A., Shen, A.H., Bucknum, M., and Chou, I-M. (1993) A new diamond anvil cell for hydrothermal studies to 2.5 GPa and from  $-190$  to  $1200$  °C. *Reviews of Scientific Instruments*, 64, 2340–2345.
- Bodnar, R.J. (1994) Synthetic fluid inclusions. XII. Experimental determination of the liquidus and isochores for a 40 wt.%  $H_2O$ -NaCl solution. *Geochimica et Cosmochimica Acta*, 58, 1053–1063.
- Bodnar, R.J. and Bethke, P.M. (1984) Systematics of stretching of fluid inclusions I: Fluorite and sphalerite at 1 atmosphere confining pressure. *Economic Geology*, 79, 141–161.
- Bodnar, R.J. and Sterner, S.M. (1985) Synthetic fluid inclusions in natural quartz. II. Application to PVT studies. *Geochimica et Cosmochimica Acta* 49, 1855–1859.
- (1987) Synthetic fluid inclusions. In G.C. Ulmer and H.L. Barnes, Eds., *Hydrothermal Experimental Techniques*, p. 423–457. Wiley, New York.
- Bodnar, R.J., Burnham, C.W., and Sterner, S.M. (1985) Synthetic fluid inclusions in natural quartz. III. Determination of phase equilibrium properties in the system  $H_2O$ -NaCl to  $1000$  °C and 1500 bars. *Geochimica et Cosmochimica Acta*, 49, 1861–1873.
- Bodnar, R.J., Binns, P.R., and Hall, D.L. (1989) Synthetic fluid inclusions. VI. Quantitative evaluation of the decrepitation behavior of fluid inclusions in quartz at one atmosphere confining pressure. *Journal of Metamorphic Geology*, 7, 229–242.
- Chou, I-M., Shen, A.H., and Bassett, W.A. (1994) Applications of the hydrothermal diamond-anvil cell in fluid inclusion research. In B. De Vivo and M.L. Frezzotti, Eds., *Fluid Inclusions in Minerals, Methods and Applications*, p. 215–230. Virginia Tech., Blacksburg.
- Dahan, N., Couty, R., and Guilhaumou, N. (1986) A one kilobar pressure heating stage: Application to the study of fluid inclusions in fluorite under confining pressure. *Physica*, 139 and 140B, 841–844.
- Fournier, R.O. and Potter, R.W. (1982) An equation correlating the solubility of quartz in water from  $25$  ° to  $900$  °C at pressures up to 10,000 bars. *Geochimica et Cosmochimica Acta*, 46, 1969–1973.
- Haar, L., Gallagher, J.S., and Kell, G.S. (1984) *NBS/NRC Steam Tables: Thermodynamic and Transport Properties and Computer Programs for Vapor and Liquid States of Water in SI Units*, 320 p. Hemisphere Publishing Corporation, Washington, D.C.
- Hosieni, K.R., Howald, R.A. and Scanlon, M.W. (1985) Thermodynamics of the lambda transition and the equation of state of quartz. *American Mineralogist*, 70, 782–793.
- Larson, L.T., Miller, J.D., Nadeau, J.E., and Roedder, E. (1973) Two sources of error in low temperature inclusion homogenization determination, and corrections on published temperatures for the East Tennessee and Laisvall deposits. *Economic Geology*, 68, 113–116.
- Poirier, J.-P. (1985) *Creep of crystals*. Cambridge University Press, Cambridge, U.K.
- Poland, E.L. (1982) *Stretching of fluid inclusions in fluorite at confining pressures up to 1 kbar*, 90 p. M.S. thesis, University of California, Berkeley.
- Rimstidt, J.D. (1997) Quartz solubility at low temperatures. *Geochimica et Cosmochimica Acta*, 61, 2553–2558.
- Roedder, E. (1984) Fluid Inclusions. In *Mineralogical Society of America Reviews in Mineralogy*, 12, 646.
- Schmidt, C. (1997) *Experimental study of the PVTX properties in part of the ternary system  $H_2O$ -NaCl- $CO_2$* , 60 p. Ph.D. dissertation, Virginia Tech., Blacksburg.
- Schmidt, C., Rosso, K.M., and Bodnar, R.J. (1995) Synthetic fluid inclusions: XIII. Experimental determination of PVT properties in the system  $H_2O + 40$  wt% NaCl + 5 mol%  $CO_2$  at elevated temperature and pressure. *Geochimica et Cosmochimica Acta*, 59, 3953–3959.
- Shen, A.H., Bassett, W.A., and Chou, I-M. (1993) The  $\alpha$ - $\beta$  quartz transition at high temperatures and pressures in a diamond-anvil cell by laser interferometry. *American Mineralogist*, 78, 694–698.
- Sterner, S.M. and Bodnar, R.J. (1984) Synthetic fluid inclusions in natural quartz. I: Compositional types synthesized and applications in experimental geochemistry. *Geochimica et Cosmochimica Acta*, 48, 2659–2668.
- (1989) Synthetic fluid inclusions. VII. Reequilibration of fluid inclusions in quartz during laboratory-simulated metamorphic uplift. *Journal of Metamorphic Geology*, 7, 243–260.
- (1991) Synthetic fluid inclusions. X: Experimental determination of P-V-T-X properties in the  $CO_2$ - $H_2O$  system to 6 kb and 700 °C. *American Journal of Science*, 291, 1–54.
- Tugarinov, A.I. and Naumov, V.B. (1970) Dependence of the decrepitation temperature of minerals on the composition of their gas-liquid inclusions and hardness. *Doklady Akademii Nauk SSSR*, 195, 112–114 (in Russian).
- Vityk, M.O. and Bodnar, R.J. (1995) Do fluid inclusions in high grade metamorphic terranes preserve peak metamorphic density during retrograde decompression? *American Mineralogist*, 80, 641–644.
- (1997) Fluid inclusions: Novel micro-strain indicators. *International Conference on Deformation Mechanisms in Nature and Experiment*, Basel, Switzerland, March 17–19, 1997, Abstract Volume, p. 35.
- Vityk, M., Bodnar, R.J., and Dudok, I. (1995) Natural and synthetic re-equilibration textures of fluid inclusions in quartz (Marmarosh Diamonds): Evidence for refilling under conditions of compressive loading. *European Journal of Mineralogy*, 7, 1071–1087.
- Vityk, M.O., Bodnar, R.J., and Schmidt, C. (1994) Fluid inclusions as tectonothermobarometers: Relation between pressure-temperature history and reequilibration morphology during crustal thickening. *Geology*, 22, 731–734.
- Werre, R.W. Jr., Bodnar, R.J., Bethke, P.M., and Barton, P.B. Jr. (1979) A novel gas-flow fluid inclusion heating/freezing stage (abstr.). *Geological Society of America Abstracts with Programs*, 11, 539.
- Zhang, Y. (1997) Mechanical and phase equilibrium in inclusion-host systems. *Eos, Transactions*, 78, S334.
- (1998) Mechanical and phase equilibria in inclusion-host systems. *Earth and Planetary Science Letters*, 157, 209–222.

MANUSCRIPT RECEIVED MAY 19, 1997

MANUSCRIPT ACCEPTED APRIL 11, 1998

PAPER HANDLED BY CRAIG MANNING